Fabrication and functionality of porous fibers prepared from microbial polyesters

Taizo Kabe*, Taku Omura*, Sakura Tsujimoto* and Tadahisa Iwata*

Abstract

This study investigates microbially produced polyesters (polyhydroxyalkanoates, PHAs) derived from renewable resources. Drawn porous fibers were fabricated from P(3HB)-based copolymers with enhanced flexibility and processability, and their microstructures were systematically characterized. Synchrotron X-ray scattering and high-resolution 3D X-ray microscopy were employed to assess changes in higher-order structural features, including crystalline orientation, lamellar morphology, and porosity. The results indicate that fiber stretchability originates from reversible structural rearrangements. To explore potential medical applications, the ligation performance of the porous fibers was also evaluated. The fibers exhibited excellent handling characteristics, including self-ligation and the formation of smaller ligation sites, supporting their potential use as surgical sutures.

1. Introduction

In modern society, plastics are used in every aspect of our lives and have become essential materials supporting social and industrial activities. However, as environmental issues such as global warming and resource depletion become increasingly serious, there is growing awareness of the need to shift from dependence on fossil resources to more sustainable alternatives. In this context, biomass-derived plastics[(1)], which are produced from renewable biomass resources, have attracted increasing attention.

Although biomass-derived plastics are expected to play an important role in achieving sustainability, only a few have been successfully put into practical use. The main reasons are that they tend to be inferior to conventional petroleum-based plastics in mechanical and thermal properties, and that their molding processes have not yet been fully optimized, leading to high production costs. To overcome these challenges and promote practical implementation, it is necessary to improve material functionality, broaden their range of applications, and increase production volume.

Among various biomass-derived plastics, this study focuses on microbial polyesters known as polyhydroxyalkanoates (PHAs), which are synthesized and accumulated by microorganisms. In particular, this study investigates the drawing mechanism and internal porous structure of PHA fibers recently developed by our research group, which exhibit unique structural characteristics combining drawability and porosity. The results of analyses using synchrotron X-rays and high-resolution 3D X-ray microscopy are presented, with a focusing on the stretching mechanism and functionality originating from the fiber microstructure.

* Graduate School of Agricultural and Life Sciences, The University of Tokyo

2. About PHA

First, an overview of microbially produced polyesters, polyhydroxyalkanoates (PHAs)[(2)] is provided. PHA are polyesters synthesized inside microorganisms using renewable resources such as sugars and plant oils as feedstocks. After use, they are degraded into water and carbon dioxide by the action of microorganisms in the natural environment. Thus, PHAs possess the dual characteristics of being both biodegradable and bio-based, and are highly regarded as environmentally friendly and resource-circulating materials (Fig. 1). In recent years, it has been reported that PHA not only degrade in environments such as soil and rivers, but also readily biodegrade in deep-sea environments[(3)]. In addition, they exhibit crystallinity and thermoplasticity.

Among the various types of PHA, the polymer with the most representative structure is poly[(*R*)-3-hydroxybutyrate] (P(3HB)). P(3HB) exhibits high crystallinity and is therefore suitable for molding processes such as fiber and film production[(4)]. However, its melting temperature is close to its thermal decomposition temperature, which makes melt processing difficult. For this reason, in practical applications, P(3HB) copolymers—whose melting point is lowered and whose crystallinity and mechanical properties are tuned by introducing a second monomer unit—are more widely used.

In P(3HB) copolymers, increasing the comonomer fraction generally reduces crystallinity, which in turn improves processability by enhancing flexibility and drawability. This molecular-structure control enables the development of materials with properties tailored to specific applications. Our research group has produced elastic fibers formed under specific processing conditions using P(3HB) copolymers, as well as elastic porous fibers that possess both stretchability and internal porosity. We have been conducting detailed analyses of their unique mechanical and structural

characteristics[5]–[8]. In the following sections, we describe the latest findings regarding the properties and structures of these materials.

3. Elastic Fibers Fabricated from the P(3HB) Copolymer P(3HB-*co*-4HB) and Higher-Order Structural Changes during Drawing[5], [7]

The P(3HB) copolymers are known to exhibit lower strength but greater flexibility compared with the P(3HB) homopolymer. We found that applying a drawing process under crystalline conditions to the P(3HB) copolymer poly[(*R*)-3-hydroxybutyrate-*co*-4-hydroxybutyrate] (P(3HB-*co*-4HB)), followed by heat drawing, enables the fabrication of elastic fibers (Fig. 2A). Here, elasticity refers to the property in which a fiber, once drawn and subsequently unloaded, spontaneously returns to a length close to its original length. The extent to which the fiber recovers relative to the applied strain is defined as the recovery ratio *R*.

$$R=\frac{l_{\max}-l_r}{l_{\max}-l_0}\cdot 100$$

In this equation, $l_{\max}$, l_r, and l_0 represent the length of the fiber at maximum extension, the length after unloading, and the initial length before drawing, respectively. Elastic fibers are used in fishing gear, sportswear, and, more recently, in garments such as stretch jeans. Figure 2B shows a plot of existing elastic fibers as a function of their tensile strength and elongation. The recovery ratio *R* is also described.

Figure 2B also includes the fiber we developed, which exhibits mechanical properties comparable to those of the elastic fibers currently used in fishing gear. Notably, its properties even exceed those of elastic fibers used in medical surgical sutures.

Although the P(3HB-*co*-4HB) elastic fiber exhibited

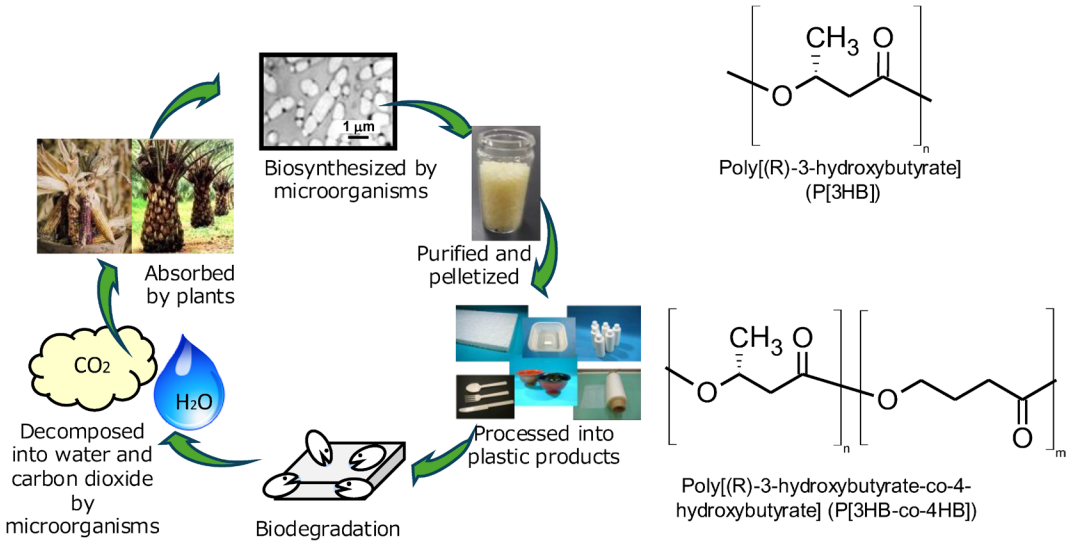

Fig. 1. Schematic illustration of the circular lifecycle of microbially produced polyesters (PHAs) and the chemical structures of poly[(*R*)-3-hydroxybutyrate] and poly[(*R*)-3-hydroxybutyrate-*co*-4-hydroxybutyrate].

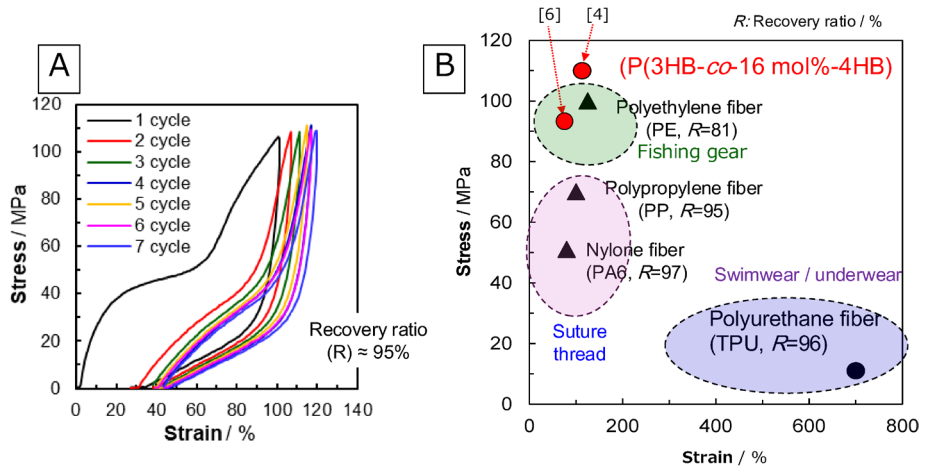

Fig. 2. (A) Cyclic tensile test results of the elastic P(3HB-*co*-4HB) fiber and (B) commercially available elastic fibers and the fiber developed in this study, plotted based on their tensile stress and strain.

excellent mechanical properties, it is necessary to clarify the mechanism by which its elasticity emerges in order to enhance its reliability as a material. Our initial hypothesis was that the system behaved like a thermoplastic elastomer, in which the P(3HB) segments function as hard segments and the second components (4HB units or 3HV units) act as soft segments. Such a structure can occur when one of the monomer units forms consecutive sequences, as in block copolymers. Therefore, we evaluated the sequence structure using ^{13}C NMR, focusing on the state of the carbonyl groups. The results revealed that the two monomer units constituting the copolymer were arranged in an essentially random manner (random copolymer), indicating that the elasticity does not originate from a block-copolymer–type mechanism[7].

Next, we considered that changes in the higher-order structure formed by crystalline and amorphous molecular chains might be responsible for the observed elasticity. Figure 3 shows the wide-angle X-ray diffraction (WAXD) patterns before and after drawing. The oriented P(3HB-*co*-4HB) fiber exhibits an orthorhombic crystal structure (α-form) (Fig. 3A). In contrast, P(3HB-*co*-4HB) fibers with higher tensile strength sometimes exhibit—in addition to the α-form—a hexagonal β-form crystal structure (Fig. 3B). In the fiber before drawing, only the oriented α-form diffraction pattern was detected, whereas after drawing, diffraction from both α-form and β-form crystals was observed. Because this structural change in the crystalline phase was detected before and after drawing, we inferred that the internal structure undergoes significant changes during deformation. To verify this, we brought the elastic fiber to a large-scale synchrotron radiation facility and performed real-time wide-angle and small-angle X-ray scattering measurements during the drawing process.

Figure 4 shows the azimuthal intensity profiles of the α(020) diffraction, the strongest reflection obtained from real-time wide-angle X-ray diffraction (WAXD) measurements during the drawing process of the P(3HB-*co*-4HB) fiber. Figure 4(a) corresponds to the drawing process and Fig. 4(b) to the relaxation process. From the azimuthal intensity profiles, the broadening of the diffraction spot can be evaluated, enabling estimation of the degree of crystalline orientation; that is, the extent to which lamellar crystals (plate-like crystals of the polymer) are aligned perpendicular to the fiber axis. The change in orientation during drawing is shown in Fig. 4(c). During drawing, the lamellar crystals exhibited a decrease in orientation, whereas upon unloading they recovered to their original orientation, demonstrating a reversible change. Based on these observations, a schematic image of the lamellar motion during drawing and relaxation is presented in Fig. 4(d). Furthermore, lattice constants calculated from the diffraction angles revealed that, during drawing, the crystal lattice was stretched in the drawing direction (i.e., along the fiber axis).

Highly oriented polymeric materials, such as fibers, are known to form a periodic stacked-lamellar structure composed of alternating plate-like lamellar crystals and amorphous chains. These stacked lamellae further develop into higher-order periodic structures. Fibers of P(3HB) copolymers are also known to possess such stacked-lamellar structures, and the periodicity of the lamellae (the long period) can be estimated from small-angle X-ray scattering (SAXS). Figure 5(a) shows the stress–strain curve during the drawing process, and Fig. 5(b) shows that during the relaxation process, together with the long periods plotted at each strain.

The long period increased from 7.8 nm before drawing to 8.8 nm at the maximum strain and returned to 7.8 nm after relaxation. Thus, similar to the changes in orientation and lattice constants, the long period expanded during drawing and returned to its original value upon relaxation. By applying an autocorrelation function to the scattering data, the lamellar crystal

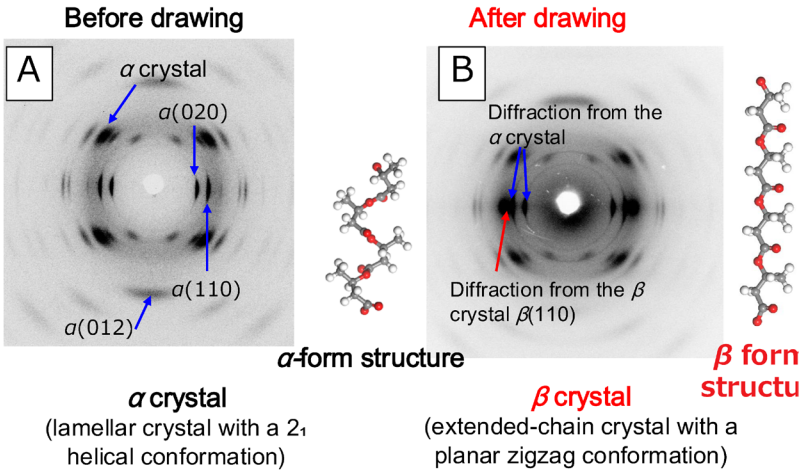

Fig. 3. Wide-angle X-ray diffraction patterns observed for fibers of P(3HB) and its copolymers. (A) Diffraction pattern originating from the oriented crystals formed in the typical α-form structure of P(3HB). (B) Diffraction pattern in which the reflections derived from the β-form—commonly observed in P(3HB) fibers with high tensile strength—appear superimposed on the α-form diffraction pattern.

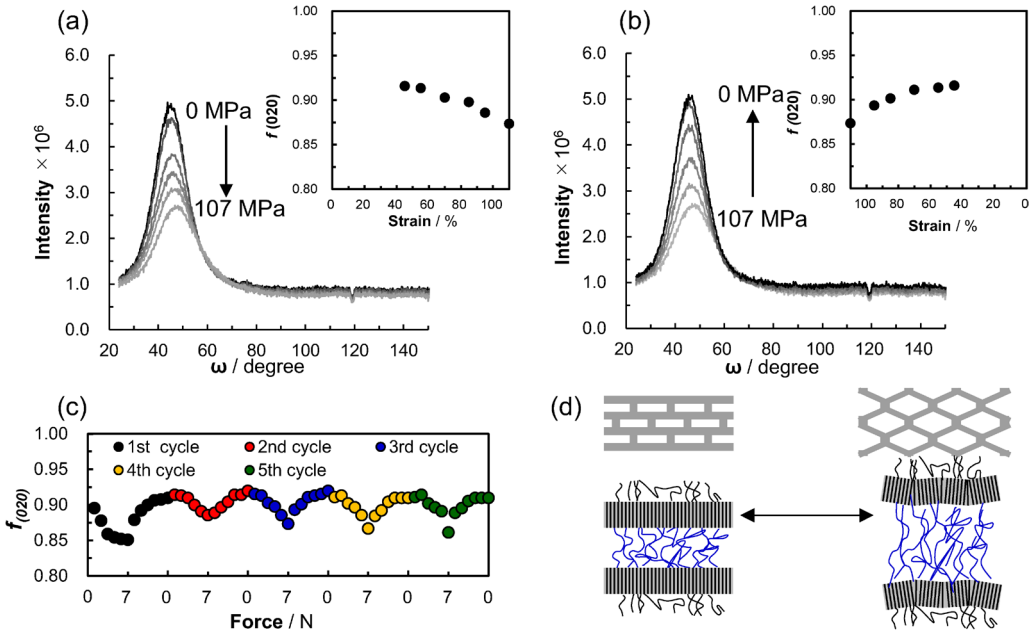

Fig. 4. Azimuthal plots of the α(020) diffraction spot of the elastic fiber. (a) Plot during the drawing process and (b) during the relaxation process. (c) Azimuthal angle changes observed during the cyclic drawing test. (d) Schematic illustration of the expected motion of lamellar crystals inferred from these results. The figure is partially modified from (7).

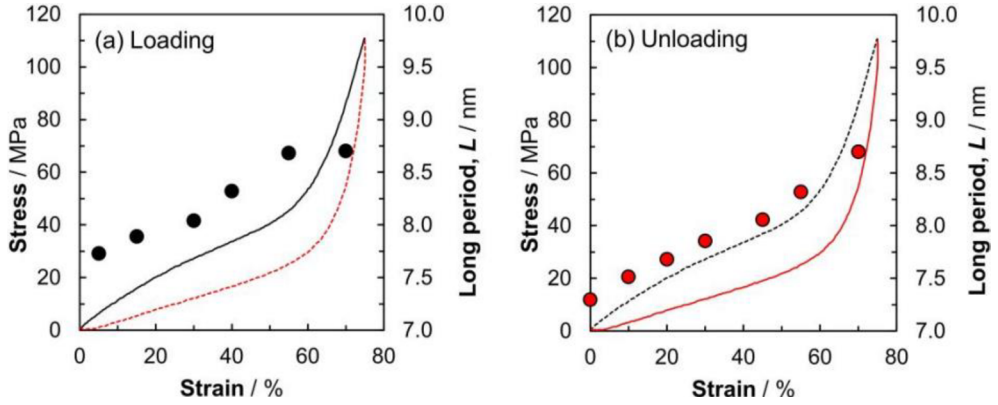

Fig. 5. Stress–strain (SS) curves during (a) the drawing process and (b) the relaxation process of the elastic fiber, together with the long period of the lamellar crystals. Adapted from (7).

thickness was also determined[9]. The lamellar thickness exhibited little change during the drawing–relaxation cycle and remained approximately 2.7 nm throughout. These results indicate that the lamellar crystals were not destroyed, and that the structure changed reversibly in accordance with the macroscopic deformation of the fiber.

Focusing on the structural changes before and after drawing, the lattice constant along the fiber axis increased by +2.5%, and the long period increased by +22%, whereas the overall macroscopic deformation of the fiber reached +70%. Although the relative contributions of the crystalline regions must be considered, even a rough estimation shows that the changes in lattice constant and long period alone cannot account for the full 70% deformation. This suggests that the amorphous regions outside the stacked lamellae, as well as higher-order structures formed by the aggregation of lamellar stacks and their spatial arrangement, undergo substantial deformation.

Taken together, these findings reveal not only the higher-order structural changes occurring during the drawing–relaxation cycle of the elastic P(3HB) copolymer fibers, but also that the driving force of elasticity originates from the reversible restoring force of the hierarchical internal structure.

4. Fabrication, Internal Structure, and Functionality of Porous Elastic P(3HB-*co*-4HB) Fibers[8]

A processing method applicable to P(3HB) and P(3HB) copolymer fibers is the microcrystal nucleation drawing method[10]. In this method, the polymer melt is rapidly quenched to below the glass transition temperature, where the molecular chains become frozen, followed by holding near the glass transition

temperature and then drawing (Fig. 6). Fibers produced by this technique are known not only to exhibit improved mechanical properties but also to form porous fibers containing numerous internal voids (pores). Several studies have reported on the pore formation mechanism, and readers are referred to those reports for further details[10]–[13].

We applied the microcrystal nucleation drawing method to the aforementioned P(3HB-*co*-4HB) and found that porous fibers with elastic properties could be produced (Hereafter, "porous fibers" in this article refer specifically to those prepared from P(3HB-*co*-4HB)). Figure 7 shows the SEM images of fibers fabricated with different holding times during the post-quenching low-temperature treatment (near the glass transition temperature, i.e., at 277 K). No pore formation was observed for holding times up to 6 h; however, coarse pores appeared when the holding time exceeded 12 h. As the holding time was further extended, the internal pore size decreased, and fibers held for 48–72 h exhibited a large number of very fine pores throughout the internal structure.

In addition, the fiber was fractured longitudinally along the fiber axis and its internal structure was

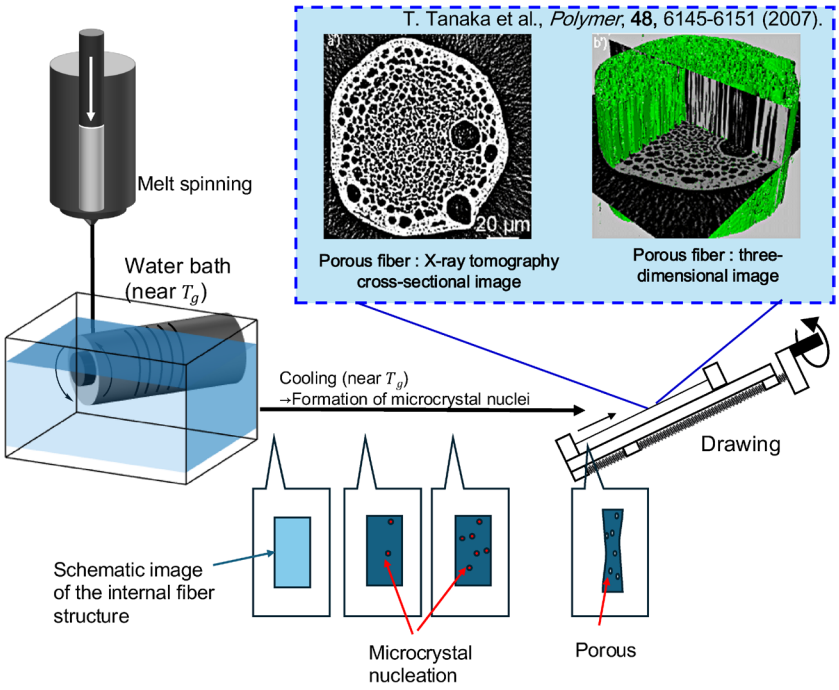

Fig. 6. Schematic of the microcrystal nucleation drawing method and structural images inside the fiber as a function of the holding time during quenching, along with the porous internal structure (upper right). The upper-right image is partially modified from (11).

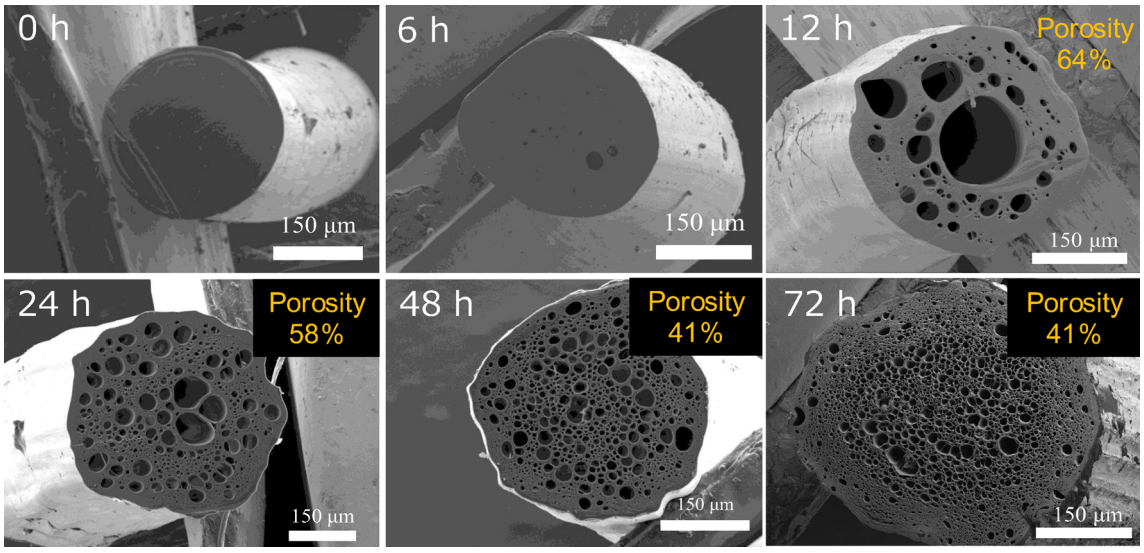

Fig. 7. Internal structural observations of the porous fibers as a function of the holding time during quenching. The figure partially uses images from (8).

examined (Fig. 8(a)). Observation of the fractured surface, together with the results obtained from the high-resolution 3D X-ray microscopy described later, revealed that the pores inside the fiber are discontinuous. Analyses of the drawing–relaxation process for this elastic porous fiber showed that the changes in lattice constants and long period before and after drawing were consistent with those described above, indicating that the stretching mechanism is essentially the same.

Furthermore, using the longitudinally fractured samples, we fabricated a small tensile fixture capable of holding the fiber during deformation and conducted SEM observations of the porous fiber cross-sections during the drawing process (Fig. 8(a)–(e)). The results demonstrated that the pores underwent deformation such that their aspect ratio increased during drawing (Fig. 8(f)). These findings suggest that, in elastic porous fibers, deformation of pores ranging from several micrometers to several hundred micrometers also contributes to the overall stretchability.

The elastic porous fiber is being considered as a candidate material for surgical sutures. This is because P(3HB-*co*-4HB) exhibits biocompatibility and P(4HB), which has a similar chemical structure, is already commercially available as a bioresorbable surgical suture. When used for suturing, the thread must be tied, a process referred to as "knotting" in medicine, and properties such as ease of tying and resistance to untying are collectively termed "knot security." For sutures, it is essential that the knot remain secure once tied, and a smaller knot size reduces the physical burden on the tissue.

In the case of elastic porous fibers, the knot tightens by itself due to elasticity after tying, and further tightening collapses the internal pores, resulting in a smaller knot. This concept was proposed by Hirata and colleagues at Nagoya University Graduate School of Medicine[14]. Figure 9 shows SEM images of the knot regions formed using the elastic porous P(3HB-*co*-4HB) fiber, the non-porous P(3HB-*co*-4HB) fiber, and the non-porous P(4HB) fiber, all tied using a surgical knot. Although the appearance differs depending on the viewing direction, the same knotting technique was used for all samples.

The knot dimensions were 1.7 mm (vertical) × 2.8 mm (horizontal) for the non-porous P(3HB-*co*-4HB) fiber and 1.2 mm × 2.3 mm for the non-porous P(4HB) fiber, whereas the elastic porous P(3HB-*co*-4HB) fiber showed much smaller dimensions of 0.9 mm × 1.3 mm. This reduction is attributed to the collapse of the pores; however, direct evaluation of the internal structure is difficult using SEM alone.

To investigate the internal structure, we employed the high-resolution 3D X-ray microscope nano3DX (Rigaku). Although this is a laboratory-based instrument, it provides exceptionally high spatial resolution, with voxel sizes below 10 μm. Figure 10 shows the measurement results for the non-porous P(3HB-*co*-4HB) fiber, the porous P(3HB-*co*-4HB) fiber, and the non-porous P(4HB) fiber. From left to right, the images represent the SEM image of the knot region, the reconstructed cross-sectional image of a region away from the knot, the reconstructed external CT view, and the reconstructed cross-sectional CT image of the fiber at the knot region.

Because this instrument reconstructs X-ray

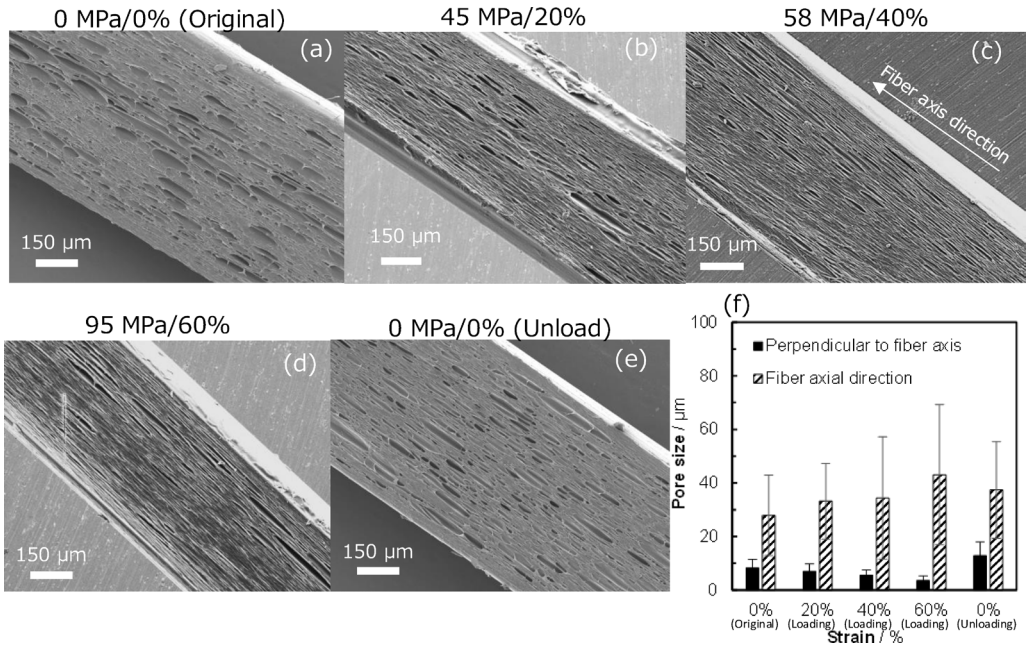

Fig. 8. SEM observations of longitudinal fracture surfaces of the elastic porous fiber. Panels (a)–(d) correspond to the drawing process, (e) shows the state after relaxation, and (f) shows the pore sizes measured from the SEM images in the directions parallel and perpendicular to the drawing direction. Reproduced from (8).

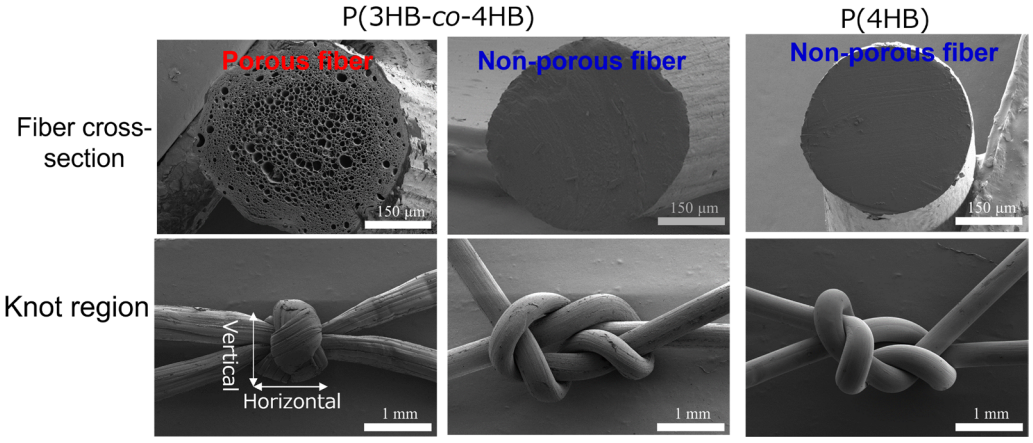

Vertical size of knot region	**0.9±0.1 mm**	1.7±0.1 mm	1.2±0.1 mm
Horizontal size of knot region	**1.3±0.1 mm**	2.8±0.3 mm	2.3±0.2 mm

Fig. 9. Knot regions and knot sizes of the elastic porous P(3HB-*co*-4HB) fiber, the non-porous P(3HB-*co*-4HB) fiber, and the non-porous P(4HB) fiber. Partially reprinted from (8).

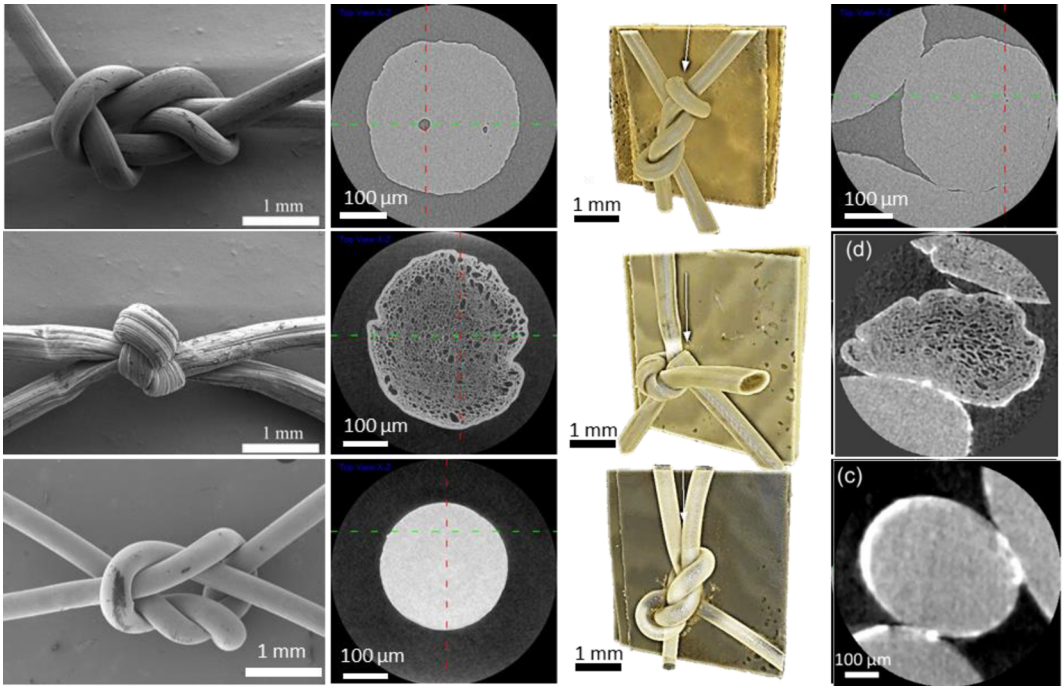

Fig. 10. SEM image of the knot region, CT cross-sectional image of the fiber before the knot, CT image of the knot region, and CT cross-sectional image of the fiber inside the knot. Reprinted from (8).

transmission images, the significant density contrast between the polymer phase and the air-filled pores enabled clear reconstruction for the porous fiber. In contrast, at the knot region—where polymer material contacts polymer material with minimal density difference—the fiber boundaries became indistinct. Following advice from researchers at the Rigaku X-ray Research Laboratory, we sputter-coated the fiber surface with a thin gold layer using an SEM coater, thereby introducing sufficient density contrast at the fiber boundaries. This approach allowed us to visualize the cross-sections of the fibers in the knot region.

Comparison of the cross-sectional shapes clearly showed that only the porous fiber exhibited marked deformation due to the collapse of pores. Figure 11 further presents (A) the reconstructed CT surface view and (B) a 3D heat map in which the resin phase is rendered transparent and the internal pores are color-coded according to size. Larger pores appear in warm colors, whereas smaller pores appear in cool colors and finally become colorless. These images revealed that most pores in the knot region were collapsed, whereas pores remained in the sections outside the knot. This behavior is also evident in the reconstructed 3D sectional image of the knot region (Fig. 11(C)).

Taken together, these results demonstrate the internal

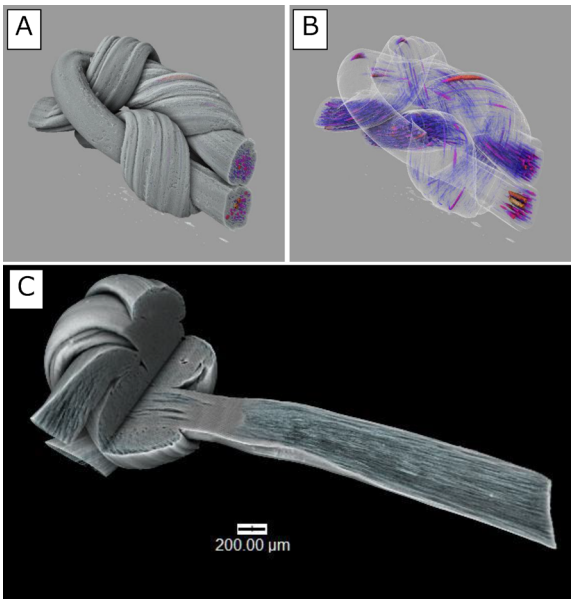

Fig. 11. Three-dimensional images reconstructed from CT data. (A) Image highlighting the surface of the knot region, (B) 3D image in which pores are color-coded according to their size and the polymer phase is rendered transparent, and (C) 3D image of the isolated knot region.

structural changes occurring in elastic porous fibers of P(3HB-*co*-4HB) during deformation, as well as the internal structural features within the knot region. These findings indicate improved knot security and highlight the potential of this material as a surgical suture.

Conclusion

Bio-based plastics have attracted considerable attention as environmentally sustainable materials; however, the manufacturing technologies and processing methods for producing these materials are not yet fully mature. Conversely, this also means that significant potential remains for discovering new functionalities and improving material properties. Such discoveries and improvements are essential for expanding applications and increasing the utilization of bio-based plastics, and advanced analytical instruments are indispensable for this type of research. Indeed, recent advancements in analytical technologies and instrument performance have begun to clarify many aspects that previously remained unresolved. Moving forward, it will be crucial to effectively leverage state-of-the-art analytical tools to advance the practical use, functionalization, and enhancement of the mechanical properties of bio-based plastics.

Acknowledgments

The P(3HB-*co*-4HB) used in this study was kindly provided by Mitsubishi Gas Chemical Company.

References

(1) T. Iwata: *Angew. Chem. Int. Ed*., **54**(11) (2015), 3210–3215.
(2) K. Sudesh, H. Abe, and Y. Doi: *Prog. Polym. Sci*., **25**(10) (2000), 1503–1555.
(3) T. Omura, N. Isobe, T. Miura, S. i. Ishii, M. Mori, Y. Ishitani, S. Kimura, K. Hidaka, K. Komiyama, M. Suzuki, K.-i. Kasuya, H. Nomaki, R. Nakajima, M. Tsuchiya, S. Kawagucci, H. Mori, A. Nakayama, M. Kunioka, K. Kamino, and T. Iwata: *Nat. Commun.*, **15**(1) (2024), 568.
(4) T. Kabe, T. Tsuge, K. Kasuya, A. Takemura, T. Hikima, M. Takata, and T. Iwata: *Macromolecules,* **45**(4) (2012), 1858–1865.
(5) T. Omura, K. Komiyama, A. Maehara, T. Kabe, and T. Iwata: *ACS Appl. Polym. Mater*., **3**(12) (2021), 6479–6487.
(6) K. Komiyama, T. Omura, T. Kabe, and T. Iwata: *Polymer*, **247**(2022), 124772.
(7) T. Omura, K. Komiyama, A. Maehara, T. Kabe, and T. Iwata: "Real-Time Structural Changes of Poly[(*R*)-3-hydroxybutyrate-*co*-4-hydroxybutyrate] Biodegradable Elastic Fibers by Using Synchrotron Radiation, Sustainable Green Chemistry in Polymer Research". Volume 1. Biocatalysis and Biobased Materials, American Chemical Society (2023), pp. 217–236.
(8) S. Tsujimoto, T. Omura, K. Komiyama, T. Kabe, A. Maehara, A. Murayama, H. Hirata, M. Suzuki, K.-i. Kasuya, D. Takahashi, and T. Iwata: *Biomacromolecules*, **25**(12) (2024), 7861–7868.
(9) G. R. Strobl, M. J. Schneider, and I. G. Voigtmartin: *J. Polym. Sci. Part B: Polym. Phys*., **18**(6) (1980), 1361–1381.
(10) T. Tanaka, M. Fujita, A. Takeuchi, Y. Suzuki, K. Uesugi, K. Ito, T. Fujisawa, Y. Doi, and T. Iwata: *Macromolecules*, **39**(8) (2006), 2940–2946.
(11) T. Tanaka, K. Uesugi, A. Takeuchi, Y. Suzuki, and T. Iwata: *Polymer*, **48**(20) (2007), 6145–6151.
(12) T. Tanaka, T. Yabe, S. Teramachi, and T. Iwata: *Polym, Degrad. Stabil*., **92**(6) (2007), 1016–1024.
(13) R. A. Rebia, K. Shizukuishi, and T. Tanaka: *Eur. Polym. J*., **134** (2020), 109808.
(14) A. Murayama, H. Yoneda, A. Maehara, N. Shiomi, and H. Hirata: *Sci. Rep.*, **13**(1) (2023), 3275.